International Journal for Innovative Engineering and Management Research
PEER REVIEWED OPEN ACCESS INTERNATIONAL JOURNAL
www.ijiemr.org

COPY RIGHT

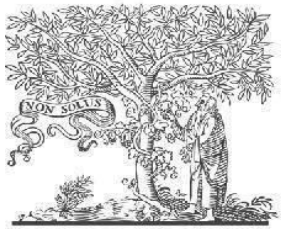

ELSEVIER SSRN

IJIEMR Transactions, online available on 4th Dec 2024. Link

https://ijiemr.org/downloads.php?vol=Volume-13&issue=issue12

DOI:10.48047/IJIEMR/V13/ISSUE12/128

Title: " EXPLORING THE STRUCTURAL, OPTICAL, THERMAL, AND NONLINEAR OPTICAL PROPERTIES OF METHYL ORANGE DYE-DOPED POTASH ALUM FOR PHOTONIC APPLICATIONS"

Volume 13, Issue 12, Pages: 623-641

Paper Authors
Shrikant Yadav, M. I. Baig

USE THIS BARCODE TO ACCESS YOUR ONLINE PAPER

To Secure Your Paper as Per UGC Guidelines We Are Providing A ElectronicBar code

International Journal for Innovative Engineering and Management Research
PEER REVIEWED OPEN ACCESS INTERNATIONAL JOURNAL
www.ijiemr.org

EXPLORING THE STRUCTURAL, OPTICAL, THERMAL, AND NONLINEAR OPTICAL PROPERTIES OF METHYL ORANGE DYE-DOPED POTASH ALUM FOR PHOTONIC APPLICATIONS.

Shrikant Yadav[1], M. I. Baig[2]

[1] Department of Physics, Prof. Ram Meghe College of Engineering and Management, Badnera, Amravati, 444701, Maharashtra, India

[1] Department of Physics, Yashwantrao Chavan College of Science Karad, Vidyanagar, Karad, 415124, Maharashtra, India.

[2]Department of Physics, Prof. Ram Meghe College of Engineering and Management, Badnera, Amravati, 444701, Maharashtra, India

shrikantyadav17@gmail.com mirza.baig@prmceam.ac.in

Abstract

For the first time, Methyl Orange (MO)-doped potash alum (PAS) single crystals of significant size were successfully grown using the slow evaporation technique at room temperature. Powder X-ray diffraction (PXRD) analysis confirmed enhanced crystallinity while retaining the cubic *Pa-3* space group. Fourier-transform infrared (FT-IR) spectroscopy verified MO incorporation, with spectral shifts indicating strong host-guest interactions. UV-Vis studies revealed a reduced band gap in the doped crystals. Thermal gravimetric and differential thermal analysis (TGA-DTA) demonstrated improved stability, with the phase transition temperature increasing for pure PAS to MO-doped PAS, attributed to hydrogen bonding and π-π stacking. The final decomposition temperature also rose from 700°C to 991°C, indicating enhanced lattice rigidity. Surface morphology analysis showed fewer defects in doped crystals, confirming superior quality. Z-scan measurements revealed a significant increase in third-order nonlinear susceptibility (χ^3: 3.1335×10^{-7} esu → 5.7571×10^{-7} esu), along with higher nonlinear refractive index (n_2) and absorption coefficient (β). These results highlight the exceptional structural, optical, thermal, and nonlinear optical properties of MO-doped PAS crystals, positioning them as promising candidates for photonic devices, nonlinear optics, and thermal sensor applications.

Keywords: PXRD, FTIR, Optical properties, Thermal Properties, Z-scan.

Introduction

Sulfate-based crystals belong to a diverse family of materials with a wide range of optical, electrical, and structural properties[1,2]. These materials are known for their excellent transparency, high thermal stability, and structural tunability, making them suitable for applications in optics and photonics. Many sulfate compounds crystallize in various structural configurations, including orthorhombic, monoclinic, and trigonal systems, which influence their nonlinear optical (NLO) behavior. Among sulfate-based crystals, compounds such as potassium liyhium sulfate (KTS), lithium sulfate monohydrate have demonstrated promising second- and third-order NLO responses[3-7] .

Inorganic materials exhibit high nonlinear coefficients, phase-matching capabilities, and efficient frequency conversion properties, making them essential in laser technology, frequency doubling (SHG), and ultrafast optical switching [8-14]. The incorporation of dopants further enhances these characteristics, improving their suitability for advanced photonic applications. Potassium aluminum sulfate (PAS) dodecahydrate, commonly known as alum ($KAl(SO_4)_2 \cdot 12H_2O$), is a widely studied sulfate crystal with notable optical properties. While it is primarily used in industrial and medicinal applications [15-20], its structural characteristics suggest the potential for nonlinear optical (NLO) behavior. Alum exhibits high transparency in the UV-Vis region, making it a suitable candidate for optical coatings and photonic devices. A water-based hydrogen bonding network in its dodecahydrate form influences its polarizability and dielectric properties, which are crucial for nonlinear optical interactions.[21-23] However, its cubic centrosymmetric structure naturally limits second-order NLO effects. To overcome this limitation, doping with organic molecules or transition metals can introduce structural distortions, breaking centrosymmetry and enhancing NLO response[24,25].

One effective approach to enhancing the nonlinear optical properties of crystalline materials is dye doping. Organic dyes possess delocalized π-electron systems, which contribute to strong polarizability and nonlinear susceptibility. When incorporated into host crystals, these dye molecules introduce new electronic transitions which increase multi-photon absorption and optical limiting properties [26-29]. Among various dyes, methyl orange (MO) is particularly notable for its strong π-electron conjugation, which significantly influences optical properties. Methyl Orange (MO) doping alters the electronic band structure, shifting the absorption edge toward the visible region, which is particularly beneficial for applications such as photonic switching and laser modulation. The azo (-N=N-) group in Methyl Orange interacts with the host material, potentially enhancing the nonlinear optical (NLO) properties.[27-32]

To the best of our knowledge, this study is the first to introduce the doping effect of Methyl Orange, an organic dye, into potash alum and explore its influence on the material's structural, optical, and nonlinear optical properties.

Characterisation Studies

The grown pure and methyl orange (MO)-doped potassium aluminum sulfate (potash alum) crystals were subjected to various characterization techniques to evaluate their structural, spectral, optical, thermal, and nonlinear optical (NLO) properties. To confirm the phase purity and crystallinity of the grown crystals, powder X-ray diffraction (PXRD) analysis was carried out using a Bruker Advance D8 diffractometer, scanning over a 2θ range of 10° to 90° with a step size of 0.08°. To study molecular vibrations and confirm the presence of functional groups, Fourier-transform infrared (FTIR) spectroscopy was performed in ATR mode using a Thermo Nicolet 380 FTIR spectrophotometer within the 400–4000 cm^{-1} range at room temperature. Optical transparency and electronic transitions of the grown crystals were analyzed using UV-Vis absorption spectroscopy, carried out on a Systronics Double Beam UV-Vis Spectrophotometer in the wavelength range of 190–1100 nm.

To assess the thermal stability, thermogravimetric analysis (TGA) and differential thermal analysis (DTA) were conducted using a Perkin-Elmer Diamond TG-DTA instrument under a nitrogen atmosphere. The nonlinear optical (NLO) properties of the grown crystals were analyzed using the Z-scan technique with a continuous-wave He-Ne laser (632.8 nm) having a beam diameter of 5 mm and a peak intensity of 93.25 kW/m². The transmittance was recorded at a finite aperture in the far field while the sample was moved along the z-axis, allowing the measurement of third-order nonlinear optical responses such as optical limiting and multi-photon absorption.

Material Synthesis and Single crystal growth:

High-quality single crystals of pure potassium aluminum sulfate dodecahydrate (PAS) (potash alum) were successfully grown using the slow evaporation solution growth technique. Merck-grade $KAl(SO_4)_2 \cdot 12H_2O$ was dissolved in double-distilled water to prepare a saturated solution. The solution was stirred continuously at room temperature until complete dissolution was achieved. To ensure purity, it was filtered using Whatman filter paper and placed in a temperature-controlled bath, where it was left undisturbed to undergo slow evaporation under controlled conditions. After five days, spontaneous nucleation occurred, resulting in the formation of high-quality seed crystals. A well-developed transparent seed crystal was carefully selected and suspended in the supersaturated solution to facilitate uniform growth. Within 12 days, a colorless, transparent single crystal of potash alum with dimensions of 15 × 15 × 10 mm³ was successfully obtained.

For the synthesis of MO-doped potash alum crystals, 1 mol% methyl orange (MO) was introduced into the saturated potash alum solution. The growth conditions remained identical to those used for pure crystals. The presence of MO influenced the crystallization process, extending the growth period. Doped crystals began forming within 10 days, and after 24 days, a well-developed MO-doped potash alum crystal with dimensions of 12 × 10 × 6 mm³ was obtained. The doped crystal exhibited a distinct coloration, confirming successful dye incorporation while maintaining structural integrity, transparency, and well-defined edges. Figures 1(a) and 1(b) depict the as-grown pure and MO-doped potash alum crystals, respectively.

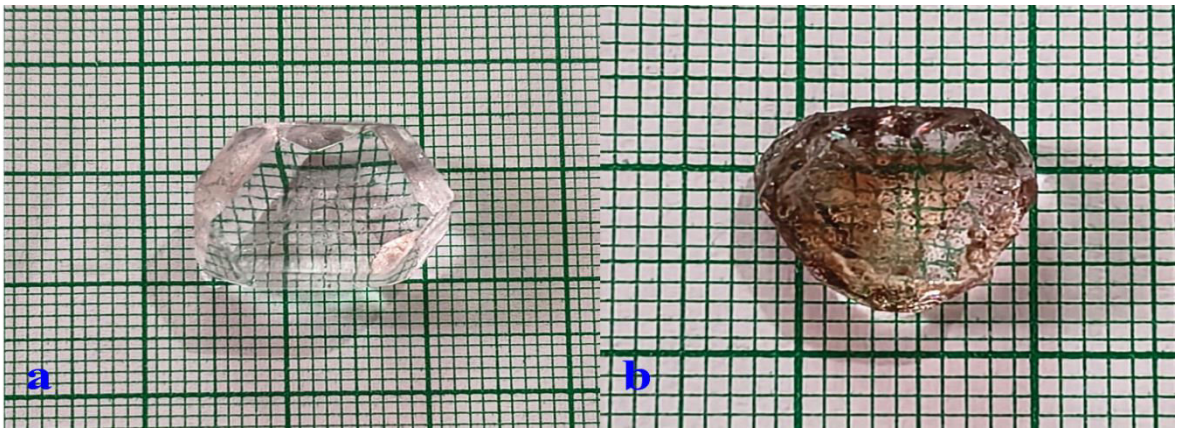

Fig. 1. a) Single Crystal Pure (PAS) b) MO-PAS

Results and Discussion

Powder X-ray diffraction (PXRD) studies

Powder X-ray diffraction (PXRD) analysis was performed to investigate the structural properties of both pure and Methyl Orange-doped potash alum crystals. The diffraction patterns of pure potash alum were compared with the reference crystallographic data from the Crystallography Open Database (COD) entry no. 1011177. The observed peaks matched well with the reference phases, confirming the identity and phase purity of the synthesized crystals. Using GSAS II software, the XRD data were analyzed to identify the crystal structure and calculate the lattice parameters for both pure and doped crystals. The powder X-ray diffraction pattern of pure potash alum and MO-doped potash alum is shown in Figure No.2 This analysis confirmed that the incorporation of Methyl Orange did not alter the fundamental crystal structure of potash alum.

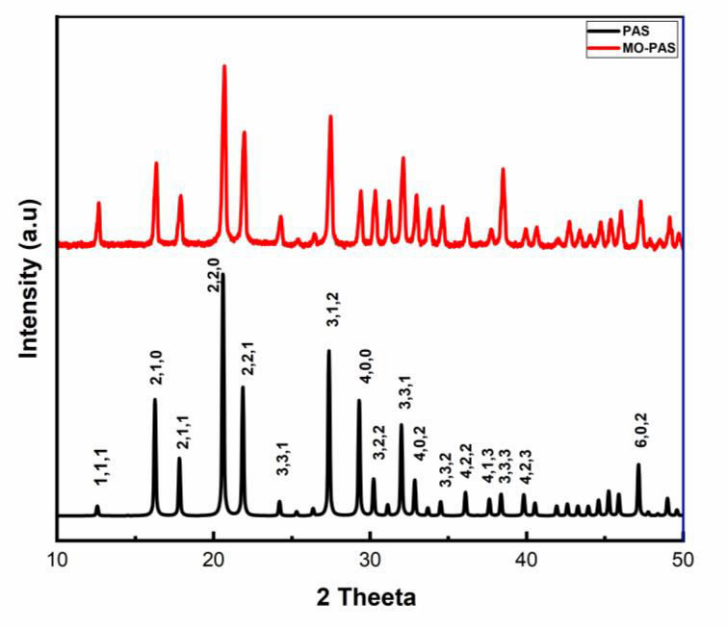

Fig. 2. X-ray powder diffraction patterns of as-grown pure and MO-doped PAS single crystals.

The lattice parameters for both pure and Methyl Orange-doped potash alum crystals were determined, and a detailed comparison of the PXRD data is presented in Table 1. The obtained diffraction pattern exhibits sharp and well-defined peaks, indicating superior crystallinity and minimal lattice strain in pure potash alum. For Methyl Orange (MO)-doped potash alum, slight peak distortions are observed, which can be attributed to lattice strain induced by the incorporation of the dopant. The low full width at half maximum (FWHM) values further confirm the high crystalline quality of the grown crystals, a critical factor for enhanced optical and electronic properties. The presence of well-defined Bragg peaks suggests uniform crystal growth and a reduction in internal defects, underscoring the high quality of the synthesized materials.

Table no.1 Lattice parameters of Pure and MO doped Potash alum.

Crystal data	PAS (Reported Work) PWXRD) [33]	PAS (Present work PWXRD)	PAS (From COD) ID: 1011177	MO-PAS (Present work PWXRD)
a (Å)	12.15	12.19	12.18	12.20
b (Å)	12.15	12.19	12.18	12.21
c (Å)	12.15	12.19	12.18	12.21
α	90	90	90	90
β	90	90	90	90
γ	90	90	90	90
Volume ($Å^3$)	1793.6	1813	1806	1821
System	Cubic	Cubic	Cubic	Cubic
Space group	Pa-3	Pa-3	Pa-3	Pa-3

A comparative structural analysis between pure and MO-doped potash alum crystals revealed that doping led to subtle modifications in lattice parameters, likely due to the incorporation of MO molecules into the crystal lattice. These minor changes suggest that the dopant slightly influences the overall unit cell dimensions while preserving the fundamental Pa-3 symmetry of the host material.

FT-IR spectral analysis

Fourier Transform Infrared (FTIR) spectrum for pure and MO-doped potash alum is shown in Figure 3. The FTIR spectrum was recorded in the range of 400–4000 cm^{-1}. The band at 3355.18 cm^{-1} corresponds to the O–H stretching vibration of water in potash alum,[15] while the peaks at 2980.70 cm^{-1} and 2887.75 cm^{-1} are attributed to C–H stretching vibrations from Methyl Orange. The symmetric and asymmetric stretching vibrations of the sulfate (SO_4^{2-}) group are observed at 1089.48 cm^{-1} and 1184.37 cm^{-1}, respectively. The significant peaks at 1681.17 cm^{-1} and 1550.86 cm^{-1} are due to the azo (–N=N–) stretching vibrations of Methyl Orange.

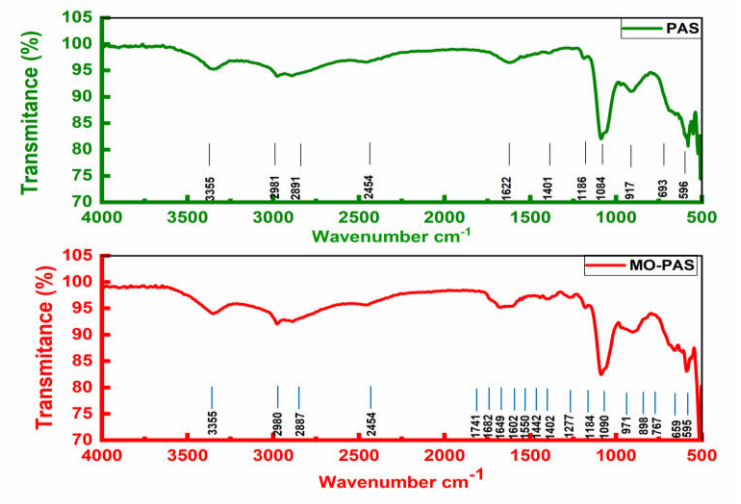

Fig. 3 FTIR spectrum for a) PAS and b) MO-PAS

The interaction between Methyl Orange and potash alum results in additional peaks, such as aromatic C=C stretching at 1602.97 cm^{-1} and C–N stretching at 1277.66 cm^{-1}, indicating successful doping. Slight shifts in peak positions and intensities, such as the O–H stretching of strongly hydrogen-bonded water molecules at 2454.47 cm^{-1} and the Al–O stretching vibration at 595.40 cm^{-1}, suggest chemical modifications caused by the incorporation of Methyl Orange into the potash alum lattice. Figure 2 shows the FTIR spectra of pure and MO-doped potash alum, and Table 2 provides the detailed vibrational band assignments. These changes provide insights into the doping process and the molecular interactions between the dopant and the host material.

Table no.2 FTIR Peak Assignments for Pure Potash Alum and MO-Doped Potash Alum

Wavenumber (cm^{-1})	Assignments for Pure Potash Alum	Assignments for MO-Doped Potash Alum
3355.18	O–H stretching vibration of water (H_2O)	Asymmetric and symmetric N-H stretching of the NH3 group, C–H stretching of the CH2 group, And O-H stretching of the hydrogen-bonded carboxyl group [30]
2980.70	P-OH stretching vibrations [30]	C–H stretching vibration of (aromatic)[34]
2887.75	P-OH stretching vibrations	C–H stretching vibration of (aromatic)
2454.47	O–H stretching of strongly hydrogen-bonded water molecules	O–H stretching of strongly hydrogen-bonded water molecules
1741.55	-	C=O stretching vibration (impurities or degradation products)
1681.17	-	Azo (–N=N–) stretching vibration of Methyl Orange
1649.96	H–O–H bending vibration of water (H_2O)	H–O–H bending vibration of water (H_2O)
1602.97	–	Aromatic C=C stretching vibration of Methyl Orange
1550.86	–	Azo (–N=N–) stretching vibration of Methyl Orange[31]
1442.47	–	Aromatic C=C stretching vibration of Methyl Orange
1402.13	–	Symmetric SO_3^- stretching vibration (Methyl Orange or alum)
1277.66	–	C–N stretching vibration of Methyl Orange
1184.37	S=O asymmetric stretching	S=O asymmetric stretching vibration of

Wavenumber (cm^{-1})	Assignments for Pure Potash Alum	Assignments for MO-Doped Potash Alum
	vibration of sulfate (SO_4^{2-})	sulfate (SO_4^{2-})
1089.48	S=O symmetric stretching vibration of sulfate (SO_4^{2-})	S=O symmetric stretching vibration of sulfate (SO_4^{2-})
971.94	S–O stretching vibration of sulfate (SO_4^{2-})	S–O stretching vibration of sulfate (SO_4^{2-})
898.18	–	Aromatic C–H out-of-plane bending vibration of Methyl Orange
767.29	O–S–O bending vibration of sulfate (SO_4^{2-})	O–S–O bending vibration of sulfate (SO_4^{2-})
659.00	O–S–O bending vibration of sulfate (SO_4^{2-})	O–S–O bending vibration of sulfate (SO_4^{2-})
595.40	Al–O stretching vibration	Al–O stretching vibration

UV VIS spectral analysis

The optical characteristics of a material play a crucial role in its potential applications in optoelectronic and photonic devices. Crystals with high transmittance and a shorter cut-off wavelength (typically in the 200–400 nm range) are preferred as they allow efficient light transmission while minimizing unwanted absorption. The UV-Vis transmittance spectra of methyl orange dye (MO), pure potash alum (PAS), and methyl orange-doped potash alum (MO-PAS) single crystals are presented in Figure 4. Methyl orange dye in aqueous solution exhibits two characteristic absorption bands: a sharp UV peak at ~228 nm (attributed to the $\pi \rightarrow \pi^*$ transition of its benzene ring) and a broad visible band between 440–465 nm (due to the $n \rightarrow \pi^*$ transition of the azo (-N=N-) group). These transitions confirm the presence of organic chromophores in the dye structure.

In the MO-PAS crystal, notable absorption peaks at 337 nm and 517 nm indicate the successful incorporation of methyl orange into the potash alum matrix. Compared to pure PAS, the doped crystal exhibits a reduction in transmittance, suggesting electronic interactions between the dye molecules and the host lattice. The transmission cut-off wavelength shifts from 216 nm (pure PAS) to 229 nm (MO-PAS), indicating modifications in the optical properties due to doping. The average transmittance in the visible region is observed to be 87% for PAS, whereas MO-PAS shows a slightly lower transmittance of 82%, confirming the influence of methyl orange on the optical transparency of the crystal.

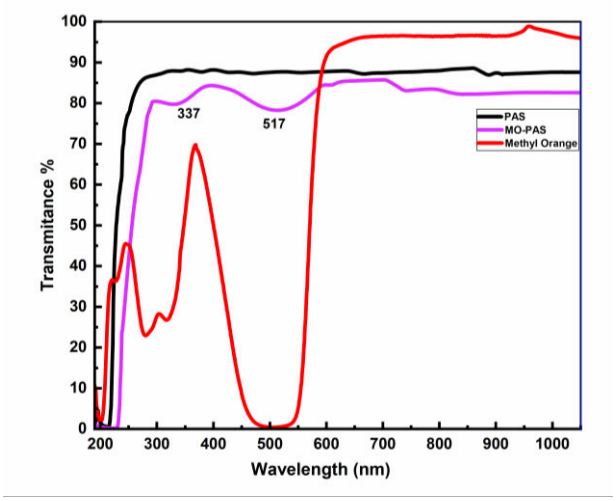

Fig. 4. UV transmission spectra for a) pure PAS and b) MO-PAS

To further analyze the optical properties, the optical absorption coefficient (α) was calculated from transmittance (T) using the relation:

$$\alpha = (2.303\ log\ (1/T))/d \qquad \ldots\ldots\ldots(1)$$

where d = 5 mm is the crystal thickness.

For direct band gap materials like potash alum crystals, the absorption coefficient (α) and photon energy (hν) follow the Tauc relation:

$$(\alpha h\nu)^2 = A(h\nu - E_g) \qquad \ldots\ldots\ldots(2)$$

where A is a constant, and Eg is the optical band gap. Tauc plots (Figure 5) were used to determine the band gaps for pure PAS and MO-PAS by extrapolating the linear portion of $(\alpha h\nu)^2$ vs. hν to the x-axis.

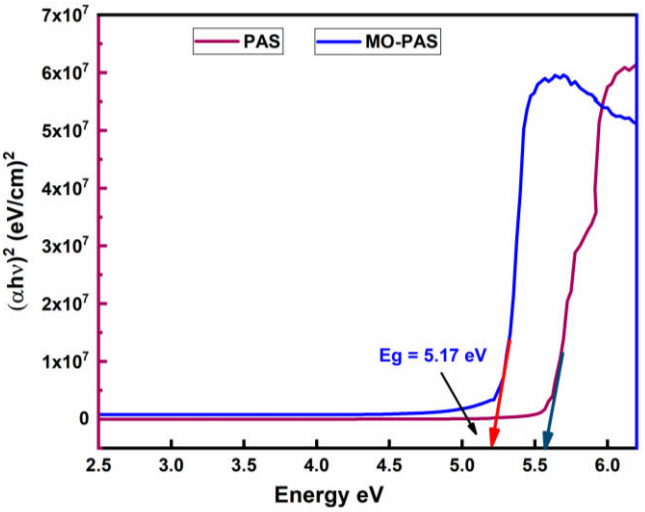

Fig. 5. Tauc's plot for a) pure PAS and b) MO-PAS

The analysis revealed a band gap of 5.60 eV for pure PAS and 5.17 eV for MO-PAS, indicating a reduction upon methyl orange incorporation. This decrease in band gap can be attributed to the introduction of additional electronic states, facilitating easier electron transitions. Similar band gap modifications have been observed in methyl orange-doped

K_2SO_4 crystals and potassium penta borate octa hydrate (MOPPB) single crystals [35,30]. The observed reduction in band gap, along with the high optical transmittance in the visible and near-IR regions, suggests that MO-PAS crystals could be potential candidates for non-linear optical (NLO) applications and photonic devices.

Thermal analysis

The thermogravimetric analysis (TGA) and differential thermal analysis (DTA) of pure PAS and MO-PAS crystals are shown in Figures 6 and 7 respectively.

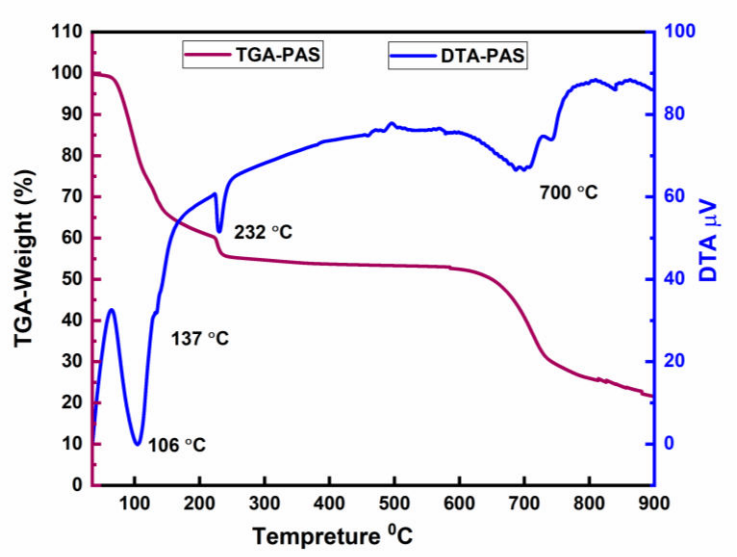

Fig. 6. TGA-DTA curve for PAS.

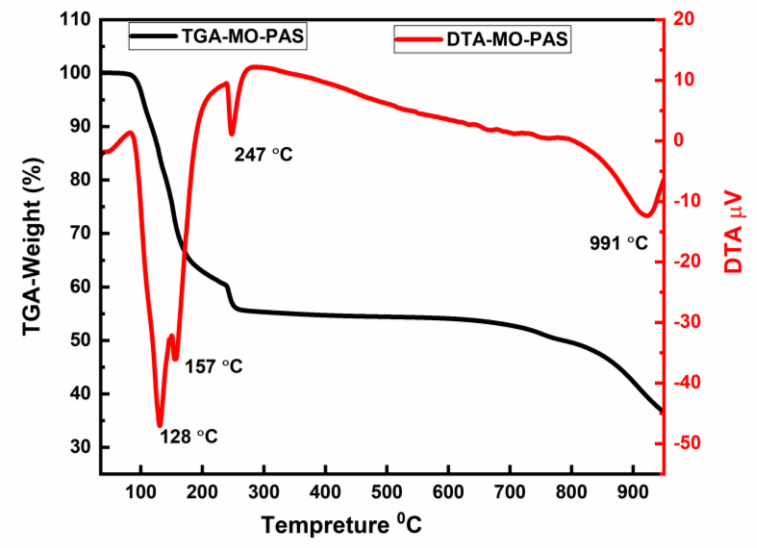

Fig. 7. TGA-DTA curve for MO-PAS.

The TGA-DTA analysis of pure PAS and MO-doped PAS crystals reveals distinct phase transitions, dehydration steps, and decomposition patterns, demonstrating the impact of MO doping on thermal behavior. In pure PAS, a structural phase transition occurs at ~106°C, whereas in MO-doped PAS, this transition shifts to 128°C, indicating that the MO molecules enhance lattice stability through additional hydrogen bonding and π-π interactions with PAS

molecules. The dehydration process in pure PAS occurs in two major steps, with the first stage involving the release of loosely bound water around 157°C, followed by the removal of tightly bound water near 247°C. In MO-doped PAS, these dehydration temperatures increase slightly, suggesting that the hydrophilic sulfonic ($-SO_3^-$) and azo (-N=N-) functional groups of MO interact with water molecules, requiring more thermal energy to break these bonds.

Upon further heating, PAS undergoes complete decomposition around 700°C, breaking down into K_2SO_4, Al_2O_3, and SO_3 gas. However, in MO-doped PAS, the final decomposition shifts to 991°C, implying enhanced thermal stability. This shift is attributed to stronger molecular interactions between MO and the PAS matrix, where the extended conjugated system of MO enhances intermolecular forces and delays lattice breakdown. The incorporation of MO not only modifies the thermal stability but also influences phase transition mechanisms, making MO-doped PAS more resistant to structural collapse at elevated temperatures. These modifications are scientifically significant, as they suggest potential improvements in thermal resilience, stability, and phase behavior, which are crucial for applications in nonlinear optics, dielectric materials, and thermal sensing technologies.

Z-Scan Analysis

The third-order nonlinear optical (NLO) properties of pure PAS and MO-PAS crystals were examined using the Z-scan technique to simultaneously determine the nonlinear refractive index (n_2) and nonlinear absorption coefficient (β). A He-Ne laser with a wavelength of 632.8 nm was used for this study. The laser beam's diameter was adjusted to 5 mm using a variable aperture before being directed onto the sample. A convex lens (f = 200 mm) was employed to focus the beam onto the sample, which had a thickness of 1 mm. The sample was mounted on a holder and moved along the Z-axis (propagation axis of the laser beam), scanning from the negative (−Z) to the positive (+Z) direction. A photodetector connected to a digital power meter was used to record the transmitted intensity through the sample. In the closed-aperture configuration, an aperture with a radius of 2 mm was used to measure the nonlinear refractive index. In contrast, for the open-aperture setup, the intensity was collected directly to determine the nonlinear absorption coefficient (β).

The open- and closed-aperture Z-scan transmittance curves of pure PAS and MO-PAS crystals are graphically represented in Figures 8a, 8b, 9a, and 9b.

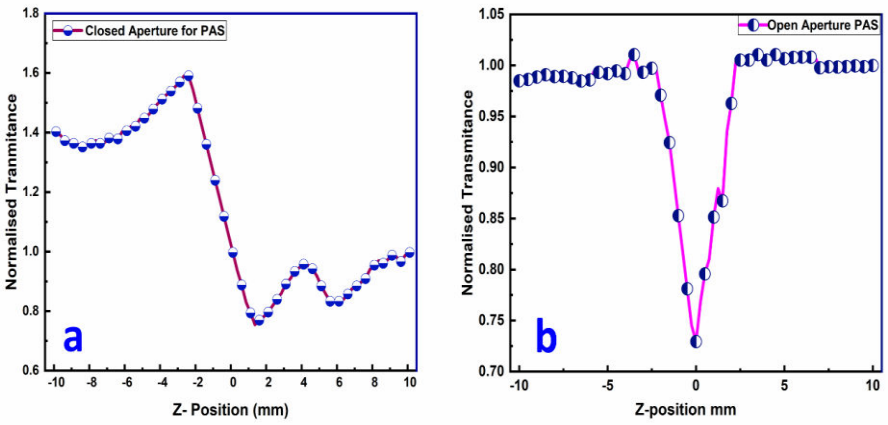

Fig. 8. a and b. Closed and Open aperture Z-scan curves of grown PAS crystal

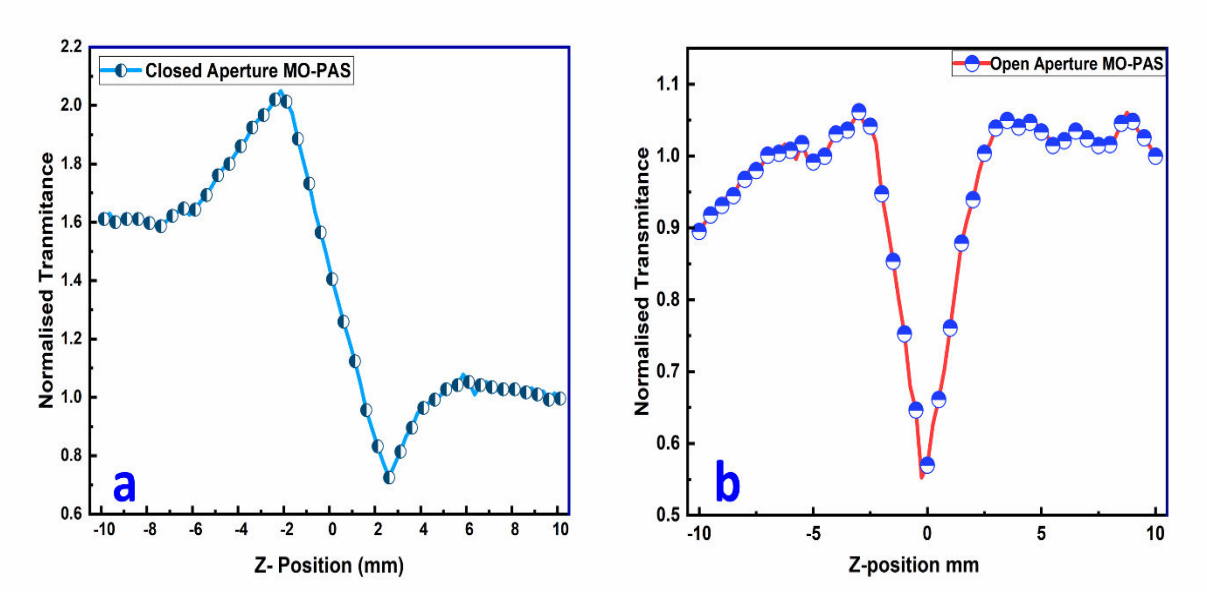

Fig. 9. a and b. Closed and Open aperture Z-scan curves of grown MO-PAS crystal

The Z-scan results of closed aperture configuration reveal a pre-focus peak followed by a post-focus valley, indicating a negative (−ve) nonlinear refractive index (n_2) for both PAS and MO-PAS. The observed self-defocusing nature is a direct consequence of the induced phase shift due to thermal lensing effects, where intense laser irradiation alters the spatial energy distribution along the crystal surface [36,37].

The negative n_2 is attributed to the influence of localized thermal accumulation from the high-intensity and repetitive He-Ne laser beam (632.8 nm), which induces variations in the refractive index. This self-defocusing property is beneficial for applications in optical limiting and all-optical switching devices.[38]

The open-aperture Z-scan data indicate the occurrence of reverse saturable absorption (RSA) in both samples, as evidenced by the reduced transmittance at the focal point compared to peripheral positions.[36] RSA suggests a dominant excited-state absorption (ESA) mechanism, where nonlinear absorption is enhanced in the excited state compared to the ground state. This phenomenon is commonly facilitated by multi-photon absorption (MPA), which leads to increase nonlinear absorption with higher light intensity. The incorporation of Methyl Orange (MO) into PAS results in a notable enhancement in the TONLO response. MO has donor ($–N(CH_3)_2$) and acceptor ($–SO_3^-$) groups, making it an intramolecular charge transfer (ICT) molecule. This means, under laser excitation, electrons can move between donor and acceptor sites, creating a strong dipole moment variation. This results in enhanced nonlinear refractive index (n_2) and reverse saturable absorption (RSA), contributing to self-defocusing behavior. These results indicate that the MO-PAS crystal exhibits superior nonlinear optical behavior, making it a promising candidate for 3D fluorescence imaging, optical switching, optical limiting, microfabrication, and frequency up conversion applications. The essential formulae required for computing n_2, β, and χ^3 are well-documented in the literature [39], and the systematically obtained values are summarized in Table 3.

Table no. 3 Third-order nlo parameters of PAS, MO-PAS crystals.

NLO parameters	PAS	MO-PAS
Laser beam wavelength (λ)	632.8 nm	632.8 nm
Optical bath length	85 cm	85 cm
Beam radius of the aperture (ωa)	4.5 mm	4.5mm
Aperture radius (ra)	2.0 mm	2.0mm
Sample thickness (L)	1.0 mm	1.0 mm
Effective thickness (Leff)	4.6674 mm	4.0816 mm
Nonlinear refractive index (n2)	3.5928×10^{-10} (m^2 / W)	6.02585×10^{-10} (m^2 / W)
Nonlinear absorption coefficient (β)	1.1538×10^{-3} (m/W)	2.1206×10^{-3} (m/W)
Real part of third-order susceptibility (Re(χ3))	1.9329×10^{-8} esu	3.2185×10^{-8} esu
Imaginary part of third-order susceptibility (Im(χ3))	3.1276×10^{-7} esu	5.7479×10^{-7} esu
Third-order nonlinear optical susceptibility (χ3)	3.1335×10^{-7} esu	5.7571×10^{-7} esu

Methyl Orange (MO) enhances the nonlinear optical (NLO) properties of Potash Alum (PAS) due to its π-conjugated system, intramolecular charge transfer (ICT), and multi-photon absorption (MPA) effects. The delocalized π-electrons in MO increase polarizability, strengthening the nonlinear refractive index (n_2) and nonlinear absorption coefficient (β). The donor ($–N(CH_3)_2$) and acceptor ($–SO_3^-$) groups facilitate charge transfer, leading to reverse saturable absorption (RSA) and self-defocusing behavior.

Correspondingly, MO doping reduces the band gap (from 5.60 eV in PAS to 5.32 eV in MO-PAS), making electronic transitions easier and further amplifying NLO effects. The local field enhancement due to dipole interactions also contributes to higher third-order optical nonlinearity (χ^3). These improvements make MO-PAS a promising material for optical switching, limiting, and photonic applications.

The $\chi(3)$ value of MO-PAS is observed to be higher compared to several other NLO crystals, as presented in Table 4.

Table no. 4 Third-order nonlinear optical comparison.

Crystal	**Third-order susceptibility ($\chi^{(3)}$)**	**References**
MO-PAS	5.7571×10^{-7} esu	Present work
CV-L-PCCM	4.826×10^{-7} esu	[40]
$MgSO_4$-SA	6.32×10^{-10} esu	[41]
KCL-SA	7.848×10^{-10}esu	[42]
KDP	3.72×10^{-14} esu	[43]

Conclusion

The bulk-sized single crystals of pure PAS and Methyl Orange (MO)-doped PAS were successfully grown using the slow evaporation solution technique at room temperature, and the influence of MO dye on various key properties was systematically investigated for the first time. Powder X-ray diffraction (PXRD) analysis confirmed that both pure and MO-doped PAS crystals retain a cubic crystal structure with the space group Pa-3, and the crystallinity of the dyed crystals was found to be enhanced. FT-IR spectroscopy revealed noticeable changes in vibrational modes, confirming the incorporation of MO dye into the PAS crystal lattice, with an enhancement in spectral intensity. UV-Vis spectroscopy showed that while MO-doped PAS exhibited lower overall transmission compared to pure PAS, it possessed a broader transmission window. The optical band gap was found to decrease from 5.65 eV for pure PAS to 5.32 eV for MO-doped PAS, indicating dye-induced modifications in the electronic structure. TGA-DTA analysis revealed distinct phase transitions, dehydration steps, and decomposition patterns, highlighting the effect of MO doping on thermal behavior. The structural phase transition observed at 106°C in pure PAS shifted to 128°C in MO-doped PAS, indicating improved lattice stability due to additional hydrogen bonding and π-π interactions between MO molecules and the PAS matrix. The dehydration process in pure PAS occurred in two major steps, with the release of loosely bound water at 157°C and tightly bound water at 247°C. In MO-doped PAS, these dehydration temperatures increased slightly due to the interaction of MO's sulfonic ($-SO_3^-$) and azo (-N=N-) functional groups with water molecules, requiring more energy to break these bonds. The final decomposition temperature increased from 970°C in pure PAS to 991°C in MO-doped PAS, demonstrating enhanced thermal stability due to the stronger molecular interactions introduced by MO doping. These modifications make MO-doped PAS more resistant to structural collapse at elevated temperatures, improving its potential for applications in nonlinear optics, dielectric materials, and thermal sensing technologies.

The nonlinear optical (NLO) properties were examined using the Z-scan technique, revealing significant enhancements due to MO doping. The nonlinear refractive index (n_2) increased from 3.5928×10^{-10} m²/W in pure PAS to 6.02585×10^{-10} m²/W in MO-doped PAS, while the nonlinear absorption coefficient (β) increased from 1.1538×10^{-3} m/W to 2.1206×10^{-3} m/W. The real ($Re(\chi^3) = 1.9329 \times 10^{-8}$ esu → 3.2185×10^{-8} esu) and imaginary ($Im(\chi^3) = 3.1276 \times 10^{-7}$ esu → 5.7479×10^{-7} esu) parts of the third-order nonlinear optical susceptibility also exhibited substantial enhancement, leading to an overall increase in χ^3 from 3.1335×10^{-7} esu (pure PAS) to 5.7571×10^{-7} esu (MO-doped PAS). These improvements suggest that MO-doped PAS possesses superior optical and NLO characteristics, making it a promising candidate for advanced photonic and optoelectronic applications.

The incorporation of Methyl Orange into PAS significantly enhances its crystallinity, optical properties, thermal stability, and nonlinear optical performance. These findings establish MO-doped PAS as a more efficient material for applications in nonlinear optics.

Acknowledgment

We sincerely thank the SAIF, IIT Madras, for providing the analytical facilities and conducting the Single Crystal X-ray Diffraction (SXRD) analysis crucial for this study. We also declare that this work was conducted without any external funding or financial support.

Conflict of Interest

The authors declare that they have no conflict of interest.

References

1. Y. Shang, J. Xu, H. Sha, Z. Wang, C. He, R. Su, X. Yang, and X. Long, Nonlinear optical inorganic sulfates: The improvement of the phase matching ability driven by the structural modulation, *Coord Chem Rev* 494, 215345 (2023). DOI: 10.1016/J.CCR.2023.215345
2. Y. Li, C. Yin, X. Yang, X. Kuang, J. Chen, L. He, Q. Ding, S. Zhao, M. Hong, and J. Luo, A Nonlinear Optical Switchable Sulfate of Ultrawide Bandgap, 3, 2298 (2021). DOI: 10.31635/CCSCHEM.020.202000436
3. R. Priya, S. Krishnan, C. Justin Raj, and S. Jerome Das, Growth and characterization of NLO active lithium sulphate monohydrate single crystals, 44, 1272 (2009). DOI: 10.1002/CRAT.200900504
4. A. Silambarasan, E. N. Rao, S. V. Rao, P. Rajesh, and P. Ramasamy, Bulk growth, crystalline perfection and optical characteristics of inversely soluble lithium sulfate monohydrate single crystals grown by the conventional solvent evaporation and modified Sankaranarayanan-Ramasamy method, *CrystEngComm* 18, 2072 (2016). DOI: 10.1039/C6CE00012F
5. K. Boopathi, P. Ramasamy, and G. Bhagavannarayana, Growth and characterization of Cu (II) doped negatively soluble lithium sulfate monohydrate crystals, *J Cryst Growth* 386, 32 (2014). DOI: 10.1016/j.jcrysgro.2013.09.028
6. H. Yadav, N. Sinha, and B. Kumar, Growth and characterization of new semiorganic nonlinear optical and piezoelectric lithium sulfate monohydrate oxalate single crystals, *Mater Res Bull* 64, 194 (2015). DOI: 10.1016/j.materresbull.2014.12.065
7. C. Amirthakumar, B. Valarmathi, P. Pandi, and R. M. Kumar, Investigation on inorganic potassium lithium sulfate single crystal grown by SR method and its characterization for nonlinear optical application, 67, 305 (2020). DOI: 10.1016/J.CJPH.2020.07.012
8. C. Ramki, and R. E. Vizhi, Insight on the growth and property studies of inorganic hydrated borate (Na6 [B4O5 (OH)4]3. 8H2O) single crystal – An effective third order nonlinear optical (NLO) material for optical limiting application, *Mater Chem Phys* 205, 138 (2018). DOI: 10.1016/J.MATCHEMPHYS.2017.11.014
9. N. Indumathi, S. Senthil, M. V. A. Raj, E. Chinnasamy, and K. Deepa, Synthesis, growth, vibrational analysis, hardness studies and theoretical calculations on inorganic NLO sulphamic acid lithium chloride single crystal, *Mater Today Proc* 50, 2636 (2022). DOI: 10.1016/J.MATPR.2020.07.591

10. S. Kavitha, and R. E. Vizhi, Studies on synthesis, structural, thermal, optical, spectral and mechanical properties of an inorganic strontium nitrate NLO single crystal, *J Mol Struct* 1276, 134746 (2023). DOI: 10.1016/J.MOLSTRUC.2022.134746
11. R. Bhatt, S. Ganesamoorthy, I. Bhaumik, A. K. Karnal, and V. K. Wadhawan, Growth rate anisotropy and absorption studies on β-BaB2O4 single crystals grown by the top-seeded solution growth technique, *Opt Mater (Amst)* 29, 801 (2007). DOI: 10.1016/j.optmat.2006.01.003
12. R. Arivuselvi, and P. R. Babu, Investigation of inorganic nonlinear optical potassium penta borate tetra hydrate (PPBTH) single crystals grown by slow evaporation method, 533, 17 (2018). DOI: 10.1016/j.physb.2017.12.051
13. S. Chidambaram, A. D. K. Raj, and R. Manimekalai, Investigation on structural, elemental, thermal, mechanical, linear, and nonlinear optical nature of potassium pentaborate tetrahydrate inorganic single crystals, *Appl Phys A Mater Sci Process* 126, 1 (2020). DOI: 10.1007/S00339-020-03605-3/METRICS
14. S. Kavitha, and R. E. Vizhi, Studies on synthesis, structural, thermal, optical, spectral and mechanical properties of an inorganic strontium nitrate NLO single crystal, *J Mol Struct* 1276, (2023). DOI: 10.1016/j.molstruc.2022.134746
15. C. Bhargava, V. K. Banga, and Y. Singh, Fabrication and Failure Prediction of Carbon-alum solid composite electrolyte based humidity sensor using ANN, 25, 773 (2018). DOI: 10.1515/SECM-2016-0272/MACHINEREADABLECITATION/RIS
16. N. Wijayati, L. R. Lestari, L. A. Wulandari, F. W. Mahatmanti, S. K. Rakainsa, E. Cahyono, and R. A. Wahab, Potassium Alum [KAl(SO4)2·12H2O] solid catalyst for effective and selective methoxylation production of alpha-pinene ether products, *Heliyon* 7, e06058 (2021). DOI: 10.1016/J.HELIYON.2021.E06058
17. A. Alisaac, M. Alsahag, M. Alshareef, R. M. Snari, M. Alhasani, H. M. Abumelha, and N. M. El-Metwaly, Development of smart cotton fabrics immobilized with anthocyanin and potassium alum for colorimetric detection of bacteria, *Inorg Chem Commun* 145, 110023 (2022). DOI: 10.1016/J.INOCHE.2022.110023
18. C. T. A. Y. Wang, and D. Lu, Study On Oral Ulcer Powder Using Temperature-Dependent X-Ray Diffraction Technique, 1, 104 (2018). DOI: 10.26480/icnmim.01.2018.104.106
19. H. Uzkul, and R. Alkan, Antimicrobial Properties of Silk Fabrics Dyed with Green Walnut Shell (Juglans regia L.), 1, 28 (2018). DOI: 10.34088/KOJOSE.410163
20. P. (2000) H. una educación eficaz para todos: L. educación inclusiva. Monográfico. educar en el 2000. mayo 2002. 15-19 Arnaiz Sánchez, www.congreso.gob.pe/comisiones/2006/discapacidad/tematico/.../inclusion.pdf, and mayo 2002 | educar en el 2000 | 15. Monográfico. HACIA UNA EDUCACIÓN EFICAZ PARA TODOS... Pilar Arnaiz Sánchez. Hacia una educación eficaz para .., Synergistic antibacterial interaction between an alum and antibiotics on some microorganism, *Sci J Med Res* 2, 47 (2018). DOI: .
21. A. M. Abdulwahab, Y. A. A. Al-magdashi, A. Meftah, D. A. Al-Eryani, and A. A. Qaid, Growth, structure, thermal, electrical and optical properties of potassium aluminum sulfate dodecahydrate (potash alum) single crystal, 60, 510 (2019). DOI: 10.1016/J.CJPH.2019.05.034

22. M. I. Miah, U. Acharjee, and L. Naheed, Optical limiting and its mechanism in potash alum, *Optik (Stuttg)* 125, 6727 (2014). DOI: 10.1016/J.IJLEO.2014.08.068
23. V. Natarajan, T. Sivanesan, and S. Pandi, Third order non-linear optical properties of potassium aluminium sulphate single crystals by Z-Scan technique, *Indian J Sci Technol* 3, (2010).
24. A. M. Abdulwahab, K. Mohammad AL-Dhabyani, A. Ahmed Ali Ahmed, N. Mohammed Al-Hada, and A. A. Qaid, The effect of lithium doping on structural, thermal, optical and electrical properties of potash alum single crystals, *Inorg Chem Commun* 145, (2022). DOI: 10.1016/j.inoche.2022.109985
25. M. Uthayakumar, V. Saraswathi, G. Pasupathi, R. Manimekalai, and V. Shinde, Structural, third-order nonlinear optical properties and optical limiting studies of novel zinc potassium aluminum sulfate nonadecahydrate single crystal, 31, 22522 (2020). DOI: 10.1007/S10854-020-04763-Z/METRICS
26. R. Saini, and D. Joseph, Optical and thermal properties of rhodamine B dye-doped sulphamic acid single crystals, 35, 1 (2024). DOI: 10.1007/S10854-024-12552-1/METRICS
27. S. Panimalar, T. Kamatchi, P. Kumaresan, S. Nithiyanantham, and R. Mohan, Second Harmonic Generation Studies on Dyes (Methyl Orange, Methyl Red) Doped Thiourea Barium Chloride (TBC) Crystals for Nonlinear Optical Applications, 5, 313 (2022). DOI: 10.1007/S42250-022-00321-8/TABLES/3
28. K. Mahendra, A. D'Souza, Ifthekarahmed, and N. K. Udayashankar, Synthesis and Optical Characterization of Amaranth Dye Doped Thiourea Barium Chloride (TBC) Single Crystals, *Mater Today Proc* 5, 16358 (2018). DOI: 10.1016/J.MATPR.2018.05.132
29. G. B. Rao, P. Rajesh, and P. Ramasamy, Enhanced optical, thermal and piezoelectric behavior in dye doped potassium acid phthalate (KAP) single crystal, *J Cryst Growth* 468, 411 (2017). DOI: 10.1016/J.JCRYSGRO.2016.11.083
30. D. Jini, M. Aravind, S. Ajitha, C. Parvathiraja, M. Muniyappan, P. A. Vivekanand, P. Kamaraj, N. Arumugam, A. I. Almansour, R. Arulnangai, R. S. Kumar, K. Perumal, and G. Gonfa, Synthesis, Growth, and Characterization of Methyl Orange Dye-Doped Potassium Sulphate Single Crystal and Its Multifaceted Activities, 2022, 4020288 (2022). DOI: 10.1155/2022/4020288
31. S. Valarmathi, K. Saravanan, and M. N. Meeran, Synthesis, growth, and characterization of methyl orange dye-doped imidazolium L-tartrate (IMLT) single crystal and its multifaceted activities, 35, 1 (2024). DOI: 10.1007/S10854-024-12384-Z/METRICS
32. K. Savitha, K. Saravanan, and K. Suganandam, Investigations on Mo dye-doped PPLT single crystals for possible non-linear optical applications, 35, 1 (2024). DOI: 10.1007/S10854-024-12486-8/METRICS
33. A. M. Abdulwahab, Y. A. A. Al-magdashi, A. Meftah, D. A. Al-Eryani, and A. A. Qaid, Growth, structure, thermal, electrical and optical properties of potassium aluminum sulfate dodecahydrate (potash alum) single crystal, 60, 510 (2019). DOI: 10.1016/J.CJPH.2019.05.034
34. A. Jagadesan, N. Sivakumar, S. Arjunan, and G. Parthipan, Growth, structural, optical, thermal and dielectric behaviour of a novel organic nonlinear optical (NLO) material: Benzimidazolium trichloroacetate monohydrate, *Opt Mater (Amst)* 109, 110285 (2020). DOI: 10.1016/J.OPTMAT.2020.110285

35. K. Kamatchi, S. Sriram, K. Sangeetha, E. Anuranjani, M. Durairaj, and T. C. Sabari Girisun, Enhanced third-order nonlinear optical properties of methyl orange dye-doped potassium penta borate octa hydrate (MOPPB) single crystals using CW diode laser for optical limiting applications, 32, 15171 (2021). DOI: 10.1007/S10854-021-06067-2/METRICS
36. S. P. Ramteke, S. Kalainathan, M. Anis, G. G. Muley, M. I. Baig, and H. Algarni, Novel report on luminescence, linear and laser induced optical traits of potassium aluminium sulphate crystal for photonic device applications, *Optik (Stuttg)* 201, 163509 (2020). DOI: 10.1016/J.IJLEO.2019.163509
37. S. Shettigar, G. Umesh, K. Chandrasekharan, and B. Kalluraya, Third order nonlinear optical properties and two photon absorption in newly synthesized phenyl sydnone doped polymer, *Synth Met* 157, 142 (2007). DOI: 10.1016/J.SYNTHMET.2007.01.003
38. W. Ji, B. Gu, and H.-T. Wang, Z-scan technique for investigation of the noninstantaneous optical Kerr nonlinearity, 34, 2769 (2009). DOI: 10.1364/OL.34.002769
39. P. Karuppasamy, V. Sivasubramani, M. S. Pandian, and P. Ramasamy, Growth and characterization of semi-organic third order nonlinear optical (NLO) potassium 3,5-dinitrobenzoate (KDNB) single crystals, *RSC Adv* 6, 109105 (2016). DOI: 10.1039/C6RA21590D
40. M. Akilan, R. Ragu, J. P. Angelena, and S. J. Das, Enhancement in mechanical, optical, SHG, photoacoustic and Z-scan studies on pure and crystal violet dye doped L-proline cadmium chloride single crystal for nonlinear optical applications, 30, 3655 (2019). DOI: 10.1007/S10854-018-00645-7/METRICS
41. J. Arumugam, M. Selvapandiyan, S. Chandran, M. Srinivasan, and P. Ramasamy, Effect of MgSO4 on sulphamic acid single crystals and their structural, optical, mechanical, thermal and third order nonlinear optical studies, *Mater Chem Phys* 242, 122479 (2020). DOI: 10.1016/J.MATCHEMPHYS.2019.122479
42. J. Arumugam, M. Selvapandiyan, S. Chandran, M. Srinivasan, and P. Ramasamy, Crystal growth, optical, thermal, laser damage threshold, photoconductivity and third-order nonlinear optical studies of KCl doped sulphamic acid single crystals, 31, 6084 (2020). DOI: 10.1007/S10854-020-03161-9/METRICS
43. R. A. Ganeev, I. A. Kulagin, A. I. Ryasnyansky, R. I. Tugushev, and T. Usmanov, Characterization of nonlinear optical parameters of KDP, LiNbO3 and BBO crystals, *Opt Commun* 229, 403 (2004). DOI: 10.1016/J.OPTCOM.2003.10.046